Elastic Properties of Nucleic Acids by Single-Molecule Force Spectroscopy

Joan Camunas-Soler,[1,2] Marco Ribezzi-Crivellari,[1,2] and Felix Ritort[1,2]

[1]Departament de Física Fonamental, Universitat de Barcelona, 08028 Barcelona, Spain; email: fritort@gmail.com

[2]CIBER-BBN de Bioingeniería, Biomateriales y Nanomedicina, Instituto de Salud Carlos III, 28029 Madrid, Spain

Annu. Rev. Biophys. 2016. 45:65–84

First published online as a Review in Advance on April 27, 2016

The *Annual Review of Biophysics* is online at biophys.annualreviews.org

This article's doi: 10.1146/annurev-biophys-062215-011158

Keywords:

DNA elasticity, force spectroscopy, single-molecule experiments, polymer biophysics, nucleic acids

Abstract

We review the current knowledge on the use of single-molecule force spectroscopy techniques to extrapolate the elastic properties of nucleic acids. We emphasize the lesser-known elastic properties of single-stranded DNA. We discuss the importance of accurately determining the elastic response in pulling experiments, and we review the simplest models used to rationalize the experimental data as well as the experimental approaches used to pull single-stranded DNA. Applications used to investigate DNA conformational transitions and secondary structure formation are also highlighted. Finally, we provide an overview of the effects of salt and temperature and briefly discuss the effects of contour length and sequence dependence.

Contents

INTRODUCTION

Single-molecule experiments are revolutionizing the way we approach biology. The ability to study single molecules offers scientists a wealth of information that was previously inaccessible. Current single-molecule techniques allow the experimentalist to track (fluorescence, imaging) and manipulate (force spectroscopy) molecules. Techniques such as single-molecule FRET (fluorescence resonance energy transfer) use fluorescent labels to unravel kinetic processes with high time resolution, and techniques such as optical tweezers make it possible to manipulate a single molecule by pulling on its ends with piconewton forces. Both types of techniques are used to characterize biochemical reactions; however, force spectroscopy mechanically perturbs single molecules to measure their response as a change in extension. In the past 20 years, researchers have used force techniques to investigate the elasticity of nucleic acids (single and double stranded) (76–78), proteins (63), and polysaccharides (53).

Direct manipulation of DNA using magnetic and optical tweezers has provided researchers an elegant way to investigate the unique physical properties of the DNA double helix and how it reacts to force, torque, and bending. The helical structure and base-stacking interactions make double-stranded DNA (dsDNA) a stiff polymer. This is in contrast with single-stranded DNA (ssDNA), which in the absence of force adopts a more compact random-coil conformation owing to its much lower (approximately 50 times) bending stiffness (**Figure 1*a***).

The different elastic properties become readily observable when a dsDNA or an ssDNA molecule is pulled from its ends (**Figure 1*b***) and a force-extension curve (FEC) is recorded. When ssDNA is stretched, the configurational entropy of the randomly coiled polymer is reduced and a force equal to a few piconewtons arises even for small end-to-end extensions (**Figure 1*b***). This entropic effect is less pronounced for dsDNA, which is stiffer than ssDNA (e.g., <0.1 pN is needed to stretch dsDNA up to 30% of its contour length, whereas 5 pN are needed to reach the same relative elongation for ssDNA). On the other hand, the double-helical structure of dsDNA imposes a much shorter contour length, leading to a rapid increase in force when it is pulled at extensions similar to its contour length (**Figure 1*b***). When a force of $\sim$65 pN is reached, the double helical structure is unraveled, in the so-called overstretching transition, and the extension of dsDNA approaches that of the single-stranded polymer (**Figure 1*a***).

The information obtained by these micromanipulation experiments has reshaped the way in which several biochemical processes are understood from a physical, biological, or technological perspective. From a biological perspective, it has changed our understanding of how DNA remodeling enzymes work (73, 80); of how DNA is compacted by nucleosome or nucleoid-like proteins in eukaryotes and prokaryotes (15, 25, 37); of how viral genomes are packaged (8, 75); and of

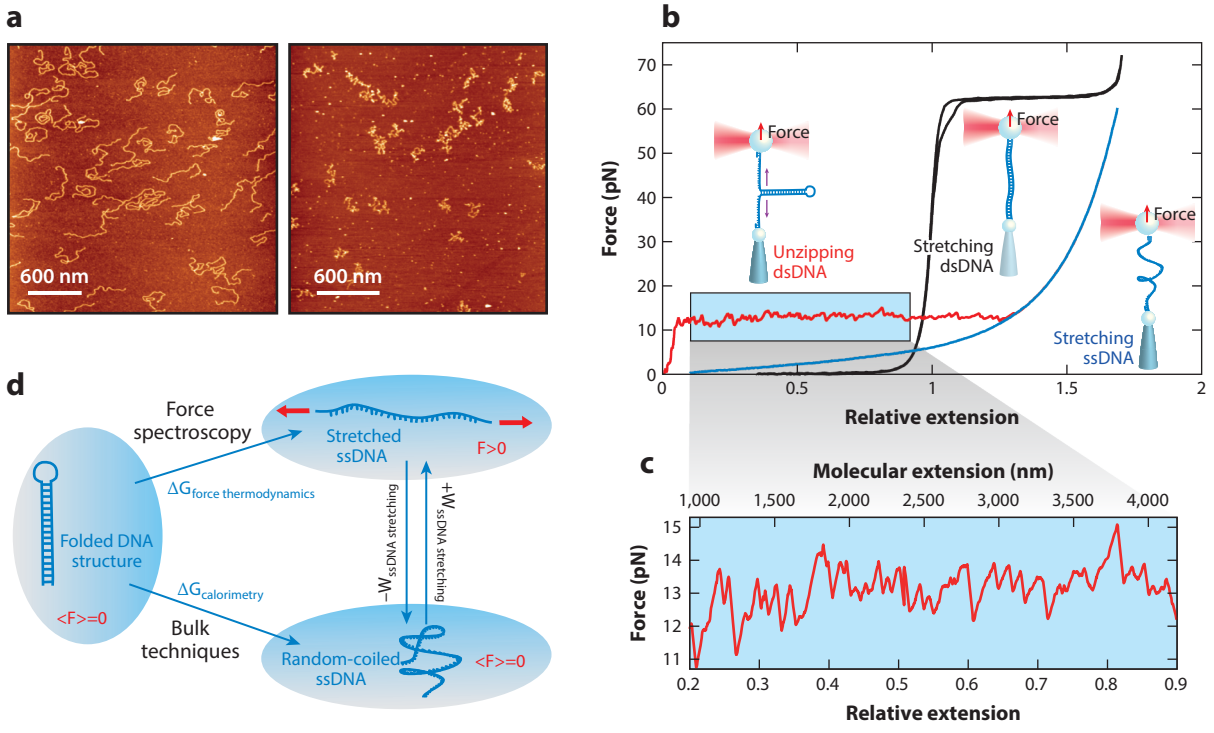

Figure 1

(*a*) Atomic force microscopy images of 2,743-bp double-stranded DNA (dsDNA) (*left*) and 2,743-bp single-stranded DNA (ssDNA) (*right*). (*b*) The force-extension curves of dsDNA stretching (*black*), ssDNA stretching (*blue*), and dsDNA unzipping (*red*). Extension is normalized to the contour length of dsDNA. (*c*) Close-up view of the unzipping pattern shaded in blue in panel *b*. Unzipping of a long DNA molecule is a multistep process. (*d*) Free energies of DNA structures measured by force thermodynamics and bulk techniques involve different final states: stretched ssDNA (*top*) and random-coiled ssDNA (*bottom*). The work required to stretch the ssDNA must be accounted for to compare both measurements.

how the mechanical properties of DNA affect replication, transcription, and repair (49, 50). From a nanotechnological perspective, elastic measurements are important for predicting the folding of oligonucleotide assemblies, such as DNA origami (46), or nucleic acid translocation through nanopores (45). In turn, the development of these technologies is providing new tools to enhance the resolution of single-molecule micromanipulation (e.g., nanofabrication of rigid handles for DNA-pulling experiments) (43, 61). From a physical perspective, a connection between the elastic properties of nucleic acids and the fundamental aspects of the physics of polyelectrolytes has been established (see 67 for a review).

Moreover, force extension measurements allow us to directly measure the mechanical work exerted on the molecule and, using statistical physics concepts, to extrapolate folding free energies, enthalpies, and entropies. We define force thermodynamics as a discipline that examines the energy processes driven by externally applied forces at the molecular scale. An accurate measurement of free-energy differences is essential to biophysics, biochemistry, and molecular biology. Weak molecular interactions in biological structures are characterized by strong enthalpy–entropy compensation effects; i.e., the contributions of both enthalpy (ΔH) and entropy ($T\Delta S$) to free energy (ΔG) are comparable, although the former is much larger than the latter. Therefore, a low

percentage error in the determination of enthalpy and entropy terms can change the overall sign of ΔG. Most thermodynamic measurements carried out in bulk (e.g., calorimetry, UV absorbance, fluorescence, or surface plasmon resonance) rest on specific assumptions (e.g., reversibility, simplified two-state models) that are not always attainable in practice. Force thermodynamics has been successfully applied in DNA-unzipping experiments with optical tweezers to obtain an improved measurement of the free energies of base pairing. When the 5′ and 3′ ends of a long DNA hairpin are pulled, it can mechanically unfold into a stretched ssDNA (**Figure 1*b***) (10, 26, 40). The process by which the two strands separate from each other (unzipping) is gradual as the optical trap moves away from the pipette; the FEC exhibits abrupt force peaks and gentle slopes in a stick-slip process (**Figure 1*c***). When approaching the trap and pipette, the hairpin gradually folds back (rezipping) into the native hairpin. If pulled sufficiently slowly, the hairpin unfolds reversibly (unzipping = rezipping) and the difference in free energy between the initial and final states equals the measured work (i.e., the area below the FEC). The FEC shows not just two states (native hairpin and fully stretched ssDNA) but many intermediates separated by variable numbers of unzipped base pairs along the curve (**Figure 1*c***).

Despite the advantages of force thermodynamics, an important caveat must be considered. Whenever a molecule is mechanically pulled, the final molecular state reached in the force spectroscopy experiment is not the same as that reached in bulk experiments. For instance, after DNA is unzipped, the final stretched conformation has much lower entropy than the random-coil state does. The total work of unfolding equals the free energy of formation of the native structure at zero force plus the work needed to stretch the ssDNA from zero force to the stretched conformation. Consequently, the folding free energies measured in force spectroscopy and bulk experiments do not match: The work required to stretch the random-coil state must be accounted for (**Figure 1*d***). For a DNA hairpin such correction is equal to the elastic work needed to reversibly stretch the ssDNA between zero force and the final force value. Therefore, a precise knowledge of the stretching free energy and of the elastic properties of the stretched polymer is mandatory. Part of the efforts to characterize in detail the elastic response of ssDNA arises from the need to subtract such energy contribution from work measurements, a key step in the accuracy of force thermodynamics.

In the sections below we review the current knowledge on the elastic properties of ssDNA derived mostly from force spectroscopy methods. When appropriate we also discuss RNA. We omit a thorough discussion of the elastic properties of dsDNA, as they have been thoroughly reviewed elsewhere (see 17, 18 for reviews), and refer to them for comparison when necessary. We address questions such as, Which model best describes the mechanical response of single-stranded nucleic acids? How can persistence length values be accurately determined? Is the elastic response sequence dependent? How do these parameters change with salt and temperature?

ELASTIC MODELS FOR DNA

The elastic rod model is the most general model that accounts for the elastic properties of linear polymers (48, 58) (**Figure 2*a***). According to this model, the energy of a linear polymer can be described by the bending energy term, $E = A\int_0^L ds(\nabla\hat{t})^2$, where A is the bending stiffness, L is the contour length, s is the one-dimensional coordinate along the polymer, and $\hat{t}(s)$ is the unit vector tangent to the polymer (**Figure 2*b***). The bending stiffness A has the dimensions of energy times length. In a thermal environment, the energy scale equals k_BT, defining a typical length scale, $L_P = A/k_BT$, called the persistence length. The persistence length sets the characteristic length scale, beyond which thermal forces randomize the direction of the polymer. For a polymer forming a semicircle of radius R, the energy equals $E = \pi A/R$, making $R \sim L_P = A/k_BT$ the typical length scale over which the polymer spontaneously bends. The correlation function $C(s) = \langle\hat{t}(0)\hat{t}(s)\rangle$

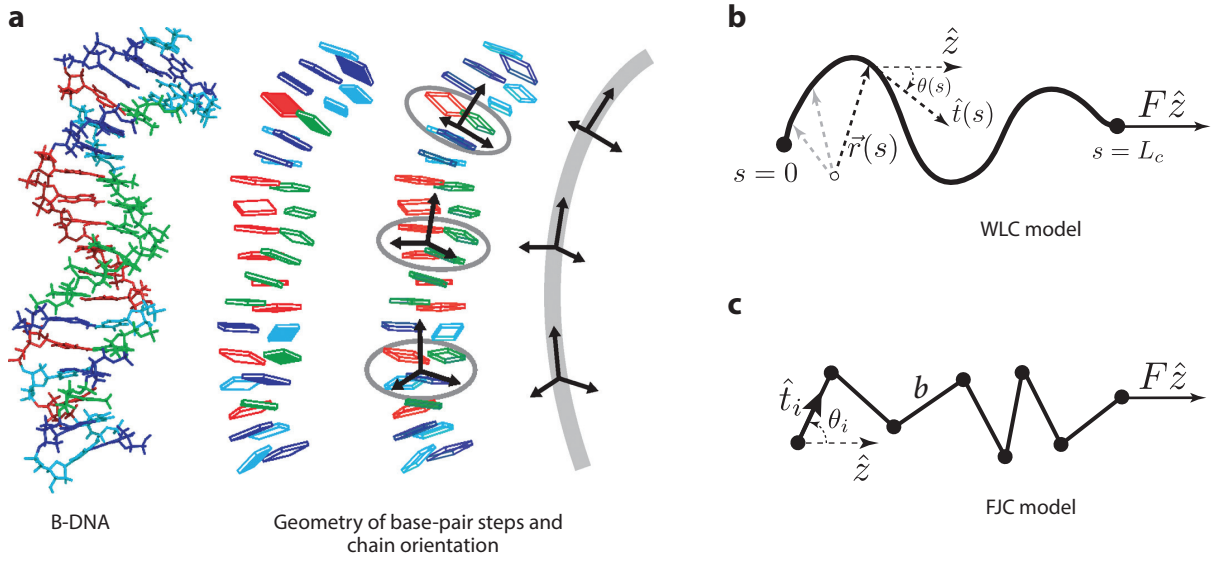

Figure 2

DNA structure and elasticity models. (*a*) DNA double-helical structure and example showing how the molecule orientation and bending stiffness reflect preferences of the base-pair sequence to assume certain geometric configurations. Modified from Reference 30 with permission. (*b*) The WLC model represents the polymer as a continuous elastic chain with a bending stiffness term. It is best suited to describe dsDNA. (*c*) The FJC is a discrete chain model describing the polymer as a sequence of uncorrelated segments of length *b*. It is best suited to describe ssDNA. Abbreviations: dsDNA, double-stranded DNA; FJC, freely jointed chain; ssDNA, single-stranded DNA; WLC, worm-like chain.

computed in this model gives $C(s) = \exp(-s/L_P)$, showing that L_P is the distance along which the tangent vector decorrelates. The average extension of the polymer along any direction vanishes owing to the rotational symmetry of the term $(\nabla\hat{t})^2$ in the energy functional. However, under the action of an externally applied force f along the x-axis, the polymer stretches, reaching a nonzero average extension $\langle x(f)\rangle$. The energy function becomes $E = A\int_0^L ds(\nabla\hat{t})^2 - fx$, with $x = \hat{x}\int_0^L ds\hat{t}(s)$ and $\hat{x}$ the unit vector along the x-axis. The model is not exactly solvable unless one goes to the discrete polymer case in which the bending and force terms in the energy function become extensive with L: The polymer L is then partitioned into N small segments of length b so that $L = Nb$, the continuum variable s is replaced by the index i, and the integral is replaced by a discrete sum (over N).

The discrete elastic rod model was introduced by Kratky & Porod in 1949 (47) and is equivalent to the one-dimensional ferromagnetic Heisenberg model in an external magnetic field (54) that can be solved via transfer matrix calculations. That solution has been exported to the polymer domain by Marko & Siggia (52), who found an interpolation formula for the thermodynamic FEC in the limits $N \to \infty$, $b \to 0$, and $L = Nb$ finite. We generically denote such FECs as $f(x)$. This model is called the worm-like chain (WLC) model: At low forces the average extension x is proportional to f, whereas at high forces x converges to L as $f^{-1/2}$. One can then devise a simple interpolating formula for $f(x)$:

$$f = \frac{k_B T}{L_P}\left(\frac{1}{4(1-x/L)^2} - \frac{1}{4} + \frac{x}{L}\right). \qquad 1.$$

Equation 1 can be modified to include the enthalpic contribution due to backbone stretching by replacing the contour length L by $L(1 + f/Y)$, where Y is the stretch modulus. This modified version is called the extensible-WLC model, whereas the standard WLC model is often called the inextensible-WLC model. Both models have been tested in optical and magnetic tweezers measurements (13, 81).

The most simple elastic polymer model, however, is the freely jointed chain (FJC) model. This model can only fit data in cases where the persistence length is comparable to the inter-monomer distance. The FJC is made of N rigid bonds of length b (the so-called Kuhn length) that can take any orientation in a three-dimensional space (**Figure 2*c***). All bond configurations carry the same energy (that can be fixed equal to zero), so the only contributor to free energy is entropy. Unlike in the WLC model, the correlation function between the orientation of bonds k and $k + i$ in the FJC model is trivial, $C(i) = \delta_{i0}$. The value of the persistence length can be obtained from the average squared end-to-end distance, $\langle R^2 \rangle = LL_k$. Comparing this value with the corresponding result for the WLC model ($\langle R^2 \rangle_{WLC} = 2L_P L$) gives the relationship $L_P = L_k/2$. When a force term is added to the FJC model, the rotational symmetry is broken and the average extension becomes equivalent to the average moment of a dipole in an external field,

$$x(f) = L\left(\coth\left(\frac{L_k f}{k_B T}\right) - \frac{k_B T}{L_k f}\right)\left(1 + \frac{f}{Y}\right). \quad 2.$$

As in the WLC model, an extensibility correction has been introduced in Equation 2 by multiplying the right hand side of Equation 2 by the term $(1 + f/Y)$, where Y is the stretch modulus.

Bustamante and colleagues (77) originally applied the FJC model to measure the elasticity of dsDNA molecules pulled with magnetic tweezers. The authors found that the extensible-FJC model cannot fit the data over all the measured range of forces. It does fit the force-extension data at low forces by assuming a contour length 20% lower than the expected value, indicating that at low forces DNA behaves as a linear spring. At the same time, if the contour length of DNA is fixed, the FJC fit overestimates the extension at a given force, indicating that $L_P \gg b$, so $L_P = b/2$ (with b on the order of the interphosphate distance) cannot be correct. The shorter apparent contour length observed by the FJC fit suggests that a bending stiffness term must contribute to expand the polymer, reaching the expected contour length at high-enough forces. In a subsequent study (76), the same authors revealed that the extensible-WLC model nicely fits the experimental data, reporting that $L_P = 50$ nm and $Y = 1000$ pN in standard conditions [for dsRNA $L_P \sim 60$ nm (1)]. **Figure 3*a*** shows all fits to the data.

Unlike dsDNA, ssDNA is much more flexible and has a lower persistence length ($L_P^{\mathrm{ssDNA}} \simeq$ 1 nm, i.e., approximately 50 times lower). Because the persistence length is similar to the interbase distance, the FJC model should better fit the ssDNA data. In 1996, Caron and colleagues (24) and Bustamante and colleagues (76) demonstrated that dsDNA overstretches at 65 pN, exhibiting a force plateau in which force-induced base-pair tilting and melting produced a new phase called S-DNA (stretched DNA). By labeling a nick-free dsDNA at both ends of the same strand, and pulling the molecule above the overstretching force in a buffer containing formaldehyde (to prevent secondary structure formation), Bustamante and colleagues could denature DNA, triggering the force-induced detachment of the unlabeled strand. In this way, they generated tethered ssDNA and measured its elastic response at various salt and pH conditions. The results showed how well ssDNA can be fit by the inextensible-FJC model up to forces of approximately 10 pN, demonstrating that entropic effects are predominant in this regime (**Figure 3*a***). Above 10 pN it is necessary to introduce the extensible-FJC model to account for stretching the phosphodiester backbone. These experiments report values of 1.5 nm and 800 pN for b (the Kuhn length) and Y (the stretch modulus), respectively (76).

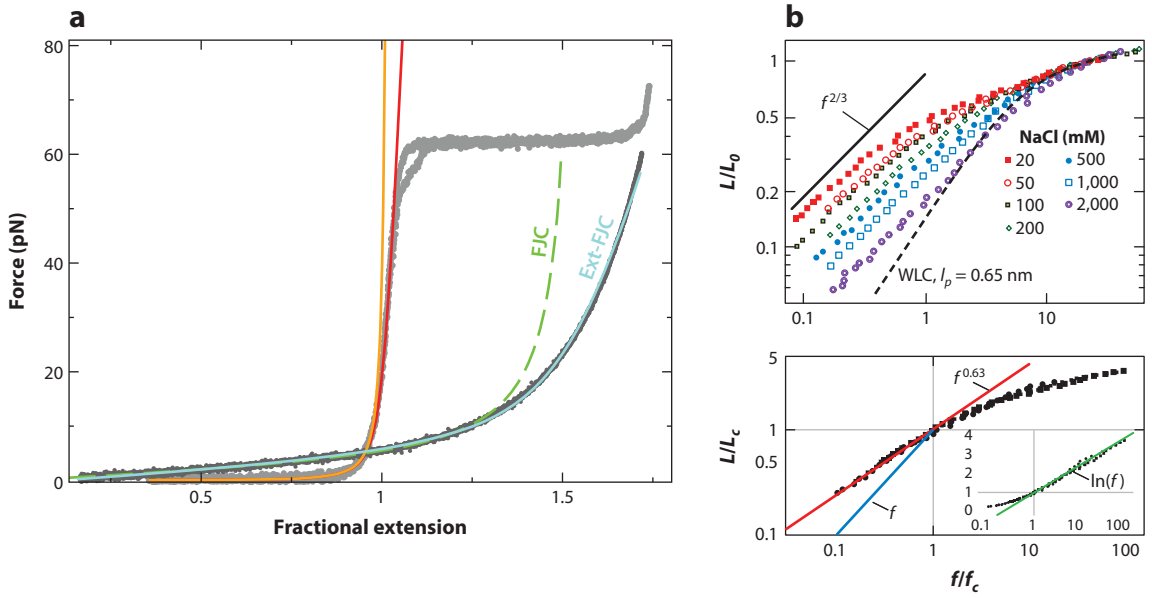

Figure 3

DNA elasticity. (*a*) The double-stranded DNA elasticity force-extension curve (FEC) (*light gray*), obtained with optical tweezers, is fit to the worm-like chain (WLC) model (*orange curve*) and the extensible-WLC model (*red curve*). Single-stranded DNA elasticity (*dark gray*) FEC is fit to the freely jointed chain (FJC) model (*green dashed curve*) and the extensible-FJC model (*cyan*). (*b*) Scaling of the FEC in the low-force region at different NaCl concentrations. Low-salt conditions show a Pincus scaling of $f^{2/3}$, which disappears at the theta point (NaCl 3 M). The lower subpanel shows the data from the upper subpanel between 20 mM and 2 M. L and f were rescaled to collapse all the data on a single master curve. The line is the power law $L \sim f^{0.63}$. In the inset the same data are plotted on lin-log axes to emphasize the logarithmic behavior at the high force. Modified from Reference 68 with permission.

When discussing the physics of polymer stretching, we must distinguish high-force from low-force regimes. These two regimes can be identified by introducing a force-dependent length scale k_BT/f, which must be compared with the Kuhn length (or equivalent Kuhn length, i.e., $L_k = 2L_P$) of the polymer. The low-force and high-force regimes are usually defined as $k_BT/f \gg \ell$ and $k_BT/f \ll \ell$, respectively. Polymer elasticity in the high-force regime can be described with either the WLC or the FJC model, depending on the kind of polymer and the salt conditions. In the low-force regime, deviations from these predictions may be expected, depending on ambient conditions, which can be interpreted using scaling concepts of polymer physics. In the case of dsDNA ($L_P = 50$ nm), the low-force regime is found below 0.04 pN and is difficult to access with current experimental approaches. For ssDNA and RNA, the low-force regime may extend up to 4 pN and is accessible with magnetic tweezers. Although magnetic tweezers grant access to low forces, optical tweezers have primarily addressed the high-force regime relevant to force thermodynamics.

A complete description of dsDNA mechanics must also account for the torsional response and the twist stretch coupling, which can be experimentally tested with magnetic tweezers or optical torque-wrench techniques (recently reviewed in 16). Notably, these techniques have been used to study torque-induced conformational transitions, such as supercoiling and torque-induced melting (32, 36), in overwound or underwound DNA.

FORCE MEASUREMENTS IN SINGLE-STRANDED DNA

Elasticity measurements on ssDNA are often challenging as compared to dsDNA. The higher flexibility of ssDNA allows the exposed nucleobases to form secondary structures through intramolecular bonding, and to nonspecifically adsorb onto surfaces, making micromanipulation complex. Consequently, most single-molecule results for ssDNA elasticity were initially derived from FRET measurements using short oligonucleotides (11, 21, 35, 57). However, in the past two decades, two main approaches have been developed to circumvent these difficulties: those that preserve the formation of nonspecific secondary structures, and those that inhibit them to show the ideal elastic behavior of the polyelectrolyte chain.

Initial optical tweezers experiments with ssDNA have exploited the ease of synthesizing and manipulating dsDNA. Indeed, the most direct method to obtain an ssDNA tether is to denature a dsDNA molecule labeled at both ends of the same strand. Denaturation can be achieved by chemically treating the sample (e.g., with NaOH or formaldehyde) or by force-induced melting dsDNA at forces above 65 pN (29, 68, 76). The latter method has been reviewed recently and the authors determined its usefulness for generating ssDNA templates of arbitrary sequence and length (**Figure 4*a***) (20). Alternative methods have used the enzymatic activity of exonucleases to create dsDNA–ssDNA hybrids (41). Chemical and enzymatic methods require careful washing of the chamber to remove denaturants once the ssDNA is generated. Force-induced melting methods apply forces that are not accessible to all force spectroscopy setups, and use labeling methods that create strong tethers between DNA and beads (typically achieved by using a biotin–streptavidin bond instead of the weaker digoxigenin–antidigoxigenin bond at both ends). Another powerful method is the oligonucleotide method (12, 51), in which a DNA hairpin is unzipped and its rezipping is prevented with a short oligonucleotide (15–30 bases) that is complementary to the loop region of the hairpin. The experiment is depicted in **Figure 4*b***. When the hairpin is fully unzipped, the oligonucleotide binds to the loop region, forming a short stretch of dsDNA that, because it is more rigid than the ssDNA, prevents rezipping at low forces. The FEC corresponds to that expected for an ssDNA, in which the number of bases is twice the number of base pairs of the hairpin.

In all the methods presented above, the ssDNA can form secondary structures (e.g., hairpins) through base-pairing and base-stacking interactions at forces below 10 pN. The classical approach to minimize the formation of such intramolecular structures is to use the aldehyde glyoxal (29). Glyoxal covalently binds to the hydrogen-bonding amine groups of ssDNA, screening intramolecular base-pairing interactions. With glyoxal ssDNA behaves as an ideal polyelectrolyte, although it can also induce intrastrand cross-links that reduce the contour length of the molecule (68).

Elasticity measurements of an ideal polyelectrolyte chain have also been performed with homopolymeric ssDNA (44) and ssRNA (71, 72), in which long polyU and polydT molecules show negligible base-pairing and base-stacking interactions (whereas polyC, polyA, and polydA form helices stabilized by base-stacking interactions). Another method for studying the ssDNA elastic response, which is applicable to short ssDNA and RNAs and proteins, is to measure the force rip or jump when a short hairpin unfolds and refolds in a pulling experiment (3). When the loop size is varied, the hairpin can unfold and refold at very different forces (**Figure 5*a***). In particular, the elastic response of the short ssDNA can be measured at very low forces (**Figure 5*b***). The FEC obtained by this method often has larger statistical errors owing to the short length of the released ssDNA; however, it also provides useful information about the contour length dependence of the elastic parameters, a current topic of interest (see Beyond Simple Elastic Models, below). The elastic response of short ssDNA molecules can also be determined by measuring the stiffness along the folded and unfolded branches of the hairpin. The difference of the inverse of

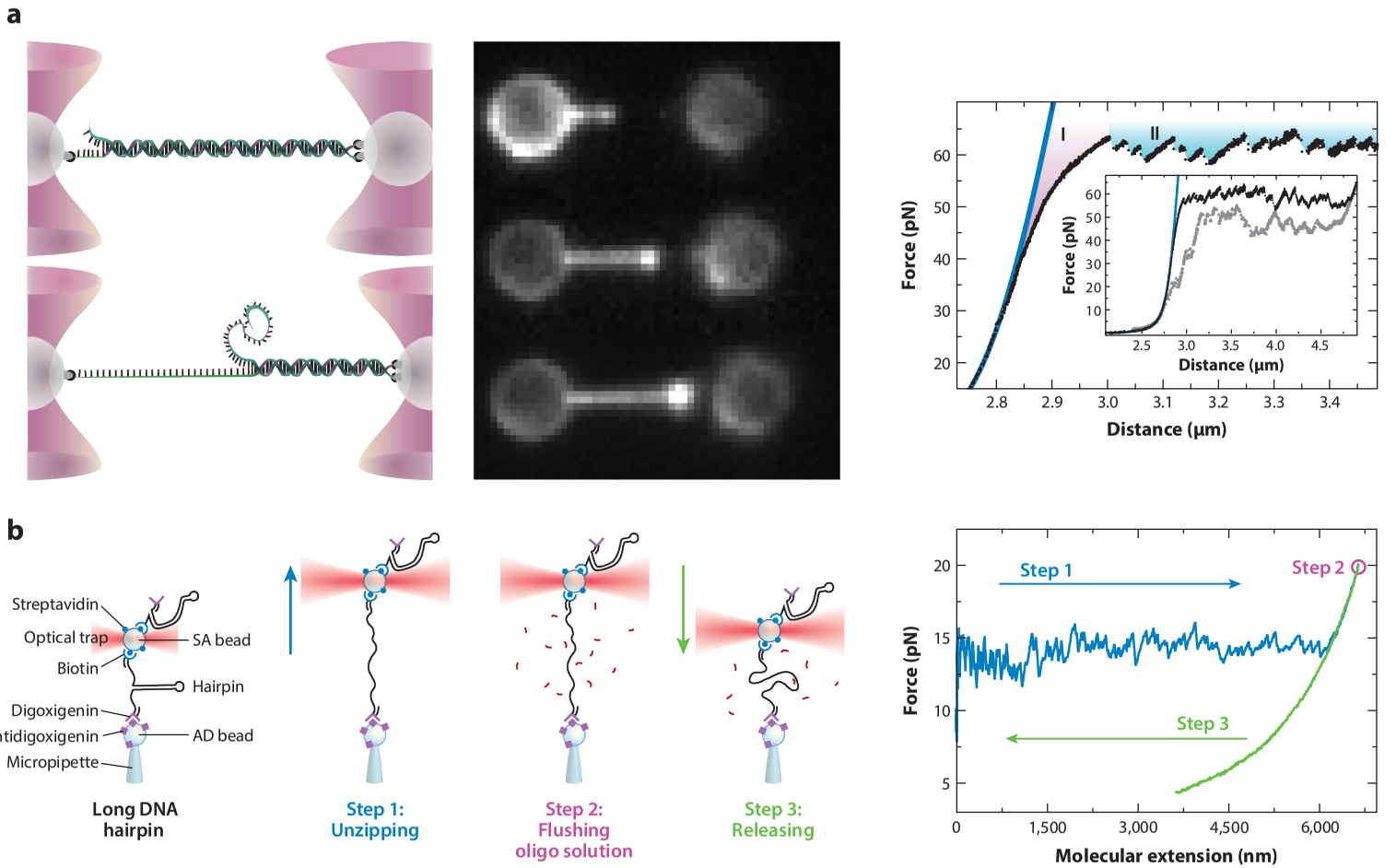

Figure 4

(*a*) *Left:* Creating an ssDNA tether using force-induced melting. The unlabeled chain is peeled off at forces above 65 pN. *Middle:* Fluorescence image showing the progression of DNA unpeeling (ssDNA is fluorescently labeled and dsDNA remains dark). *Right:* FEC of dsDNA during unpeeling (hysteresis shown in the inset is indicative of unpeeling/rehybridization). Modified from Reference 36 with permission. (*b*) *Left:* Steps to generate an ssDNA tether using the oligo method. *Right:* FEC of the different steps in the oligo method—unzipping the hairpin (*blue*), waiting for the oligo to bind during flushing (*purple*), and releasing the force to record the FEC of ssDNA (*green*). Abbreviations: AD, antidigoxigenin; dsDNA, double-stranded DNA; FEC, force-extension curve; SA: streptavidin; ssDNA, single-stranded DNA.

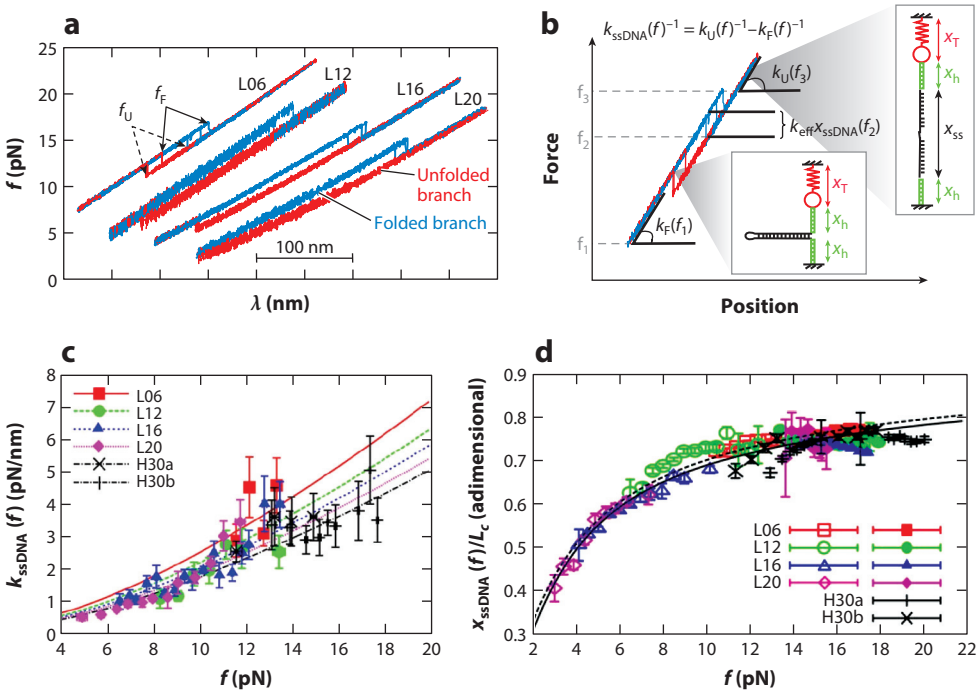

Figure 5

Measuring the elasticity of single-stranded DNA (ssDNA) oligonucleotides. (*a*) Unzipping experiments on DNA hairpins with loops of different lengths [$G(A)_n$]. (*b*) Different strategies to measure the elastic parameters of a short oligo from its force-extension curve (FEC). The slope of each branch of the FEC gives the stiffness of the molecular construct as a function of force. The stiffness of ssDNA can be computed when the stiffness of both branches is known. An alternative approach uses the force jump, which is proportional, through the effective stiffness, to ssDNA extension. The hairpin diameter in the folded configuration must be taken into account. (*c*) Elasticity measurement based on the unfolding/refolding force jumps for different loop lengths. (*d*) ssDNA stiffness estimated from FECs of short oligos.

both stiffnesses along both branches provides a measurement of the ssDNA stiffness in a wide range of forces (**Figure 5*c***) (3). Finally, CEBA (continuous effective barrier approach), which is based on dynamic force spectroscopy measurements, extracts the elastic response of ssDNA by matching the experimental kinetic barriers obtained from unfolding and folding rupture force distributions. The CEBA method has been also applied to RNAs and proteins (9). A summary of elastic measurements reported for ssDNA by different methods and elastic models is shown in **Table 1**.

THE IMPORTANCE OF SINGLE-STRANDED DNA IN CONFORMATIONAL TRANSITIONS

Detailed knowledge of the elastic response of ssDNA is essential to extract accurate information about conformational transitions in DNA from single-molecule force experiments. A prominent example is DNA unzipping (10). Huguet et al. (40) accurately determined at varying monovalent salt conditions the energies for 10 different nearest-neighbor (NN) motifs. The energies of the

Table 1 Elastic properties of ssDNA determined by different methods and models

Method	Model[a]	NaCl (M)	l_k (nm)	l_p (nm)	S (pN)	l_c (nm/base)	References
Long ssDNA force spectroscopy							
Force melting/ chemical denaturation, 48 kb and 3 kb	FJC	0.15	1.5	–	800	0.57	23, 29, 76
Oligo method, 13 kb	FJC	0.1	1.55 (4 nm)	–	630 (70 p N)	0.57[d]	12, 28[b]
Oligo method, 13 kb	WLC	1	–	0.76 (5 nm)	–	0.70 (2 nm/base)	12, 28[b]
Glyoxal denaturation, 10.5 kb	WLC	3	–	0.69 (3 nm)	–	Not reported	56, 68[c]
Short ssDNA force spectroscopy							
Short hairpins ΔF, ~20 b	WLC	1	–	1.35 (5 nm)	–	0.58 (2 nm/base)	3
Short hairpins stiffness, ~20 b	WLC	1	–	1.35 (5 nm)	–	0.58[d]	3
Short hairpins DFS, ~20 b	WLC	0.2	–	1.0–1.5	–	0.58–0.67	84
Short ssDNA FRET							
polyT 10- to 70-mers, FRET	WLC	1	–	1.6	–	0.63[d]	57
polyT 40-mers, FRET/SAXS	WLC	1	–	0.94	–	0.57[d]	21
ssRNA							
polyU ssRNA, 1.3–4 kb	WLC	0.5	–	0.80 (2 nm)	–	Not reported	71
polyU ssRNA, 4–10 kb	WLC	4	–	0.83 (5 nm)	–	0.59[d]	42
polyU ssRNA, FRET/SAXS, 40-mers	WLC	1	–	1.2	–	0.49	21
Short RNA hairpin, DFS	WLC	1	–	0.75 (5 nm)	–	0.665[d]	9

[a]To compare the WLC and FJC models $l_k \sim 2l_p$ (see section Elastic Models for DNA).
[b]The salt and temperature dependence of l_p, l_k are reported in these references.
[c]Results from experiments at low forces ($F < 5$ pN).
[d]These values are fixed parameters in the fit.
Abbreviations: DFS, dynamic force spectroscopy; FJC, freely jointed chain; FRET, fluorescence resonance energy transfer; SAX, small-angle X-ray scattering; ssDNA, single-stranded DNA; ssRNA, single-stranded RNA; WLC, worm-like chain.

nearest-neighbor motifs show heterogeneous salt corrections, the average of which is compatible with the homogeneous correction commonly assumed in the unified oligonucleotide scheme used by most web-based predictor tools (69). However, an alternative interpretation of these results attributes these heterogeneous salt corrections to the sequence dependence of the elastic response of ssDNA. The strongest deviations from the homogeneous salt correction were observed by Huguet and colleagues (40) in purine-purine and pyrimidine-pyrimidine stacks, suggesting that large differences in the elastic response might be observed in homopolymeric sequences. Sequence-dependent base-stacking effects on the elastic response of homopolymeric RNAs have been reported (44, 55, 71, 72). A clear understanding of sequence-dependent effects is still needed and future unzipping experiments with homopolymeric sequences might be illuminating.

The same conclusion applies to free-energy measurements of DNA native structures, kinetic intermediates, and misfolded structures (2). An exact estimation of the parameters of ssDNA elasticity improves the accuracy of predicting the free energy in all cases. The same holds true for mechanically unfolded RNAs and proteins.

The contribution of the elastic response is also important for other conformational transitions such as the B-S transition in DNA, which occurs at a force of approximately 65 pN. This high force makes the stretching energy especially important to reliably estimate the free energy difference across the B-S transition (33, 34, 36).

SALT AND TEMPERATURE DEPENDENCE

The elastic response of nucleic acids depends on both salt and temperature. In fact, DNA and RNA are strongly charged polyelectrolytes whose thermodynamic stability is determined largely by the effect of counterions that screen the negatively charged phosphates. In the dilute (low salt concentration) regime the Debye-Hückel theory predicts a characteristic length scale, called the Debye screening length λ_D, that defines a high-density layer of counterions beyond which the charge of the macroion or polymer is fully screened. For single-ion species the Debye length is given by the expression $\lambda_D = \sqrt{\frac{\varepsilon_0 k_B T}{c_0 q^2}}$, where ε_0 is the dielectric constant of the medium, T is the temperature, q is the electric charge of the ions, and c_0 is the ion density in bulk (with dimensions of inverse volume). This expression clearly shows the significance of temperature and ion density for determining the Debye length. Accordingly, it is assumed that the values of the elastic persistence length, L_P, and Kuhn length, L_k, directly depend on temperature and charge through the dependence exhibited by λ_D, $L_{P,K} = L^0_{P,K} + L^{\mathrm{el}}_{P,K}$, where $L^0_{P,K}$ is the intrinsic persistence or Kuhn length and $L^{\mathrm{el}}_{p,K}$ is the electrostatic contribution. In the simplest scaling scenario, the electrostatic contribution is proportional to the Debye screening length, i.e., proportional to the square root of temperature divided by the concentration of ions in solution.

The existing literature on the effect of counterion concentration on the mechanics of polyelectrolytes offers different predictions. A theory independently developed by Odijk (59) and Skolnick & Fixman (74) (OSF) predicts a quadratic dependence of $L^{\mathrm{el}}_{p,K}$ on the Debye length. Subsequent work by Barrat & Joanny (4) has shown that the OSF prediction holds for polymers with sufficient stiffness. For flexible chains, fluctuations modify the physical scenario and the dependence of $L^{\mathrm{el}}_{p,K}$ on λ_D becomes linear. Experiments have shown how the persistence length of dsDNA conforms to the OSF prediction (6). The persistence length of dsRNA follows a trend similar to that of dsDNA (39).

Single-molecule measurements of 13.6-kb ssDNA molecules in the high-force regime (12) using the oligo method have measured the persistence and Kuhn lengths as a function of monovalent (NaCl) and divalent ($MgCl_2$) salt concentrations (**Figure 6*a***) using either the WLC or the FJC models at high enough forces (**Figure 6*b***) where the formation of the secondary structure is prevented (**Figure 6*c*,*d***). The results for both salt concentrations appear compatible with a linear dependence of $L^{\mathrm{el}}_{p,K}$ on λ_D, although data might also be fit with a quadratic dependence (OSF theory), especially for divalent salt (**Figure 7*a***). In both cases the value of the intrinsic persistence length is 0.7 nm. Interestingly, the effect of monovalent and divalent salts follows the 100th rule characteristic of nucleic acids: The nonspecific contribution of divalent cations to the free energy at a given concentration is equivalent to that of monovalent cations taken at 100-fold concentration. A similar rule holds true for the $L_{p,K}$ values for ssDNA (**Figure 7*a***). Using several monovalent and divalent salts, McIntosh & Saleh (56) obtained compatible results by analyzing the scaling behavior of the FEC in the low-force regime.

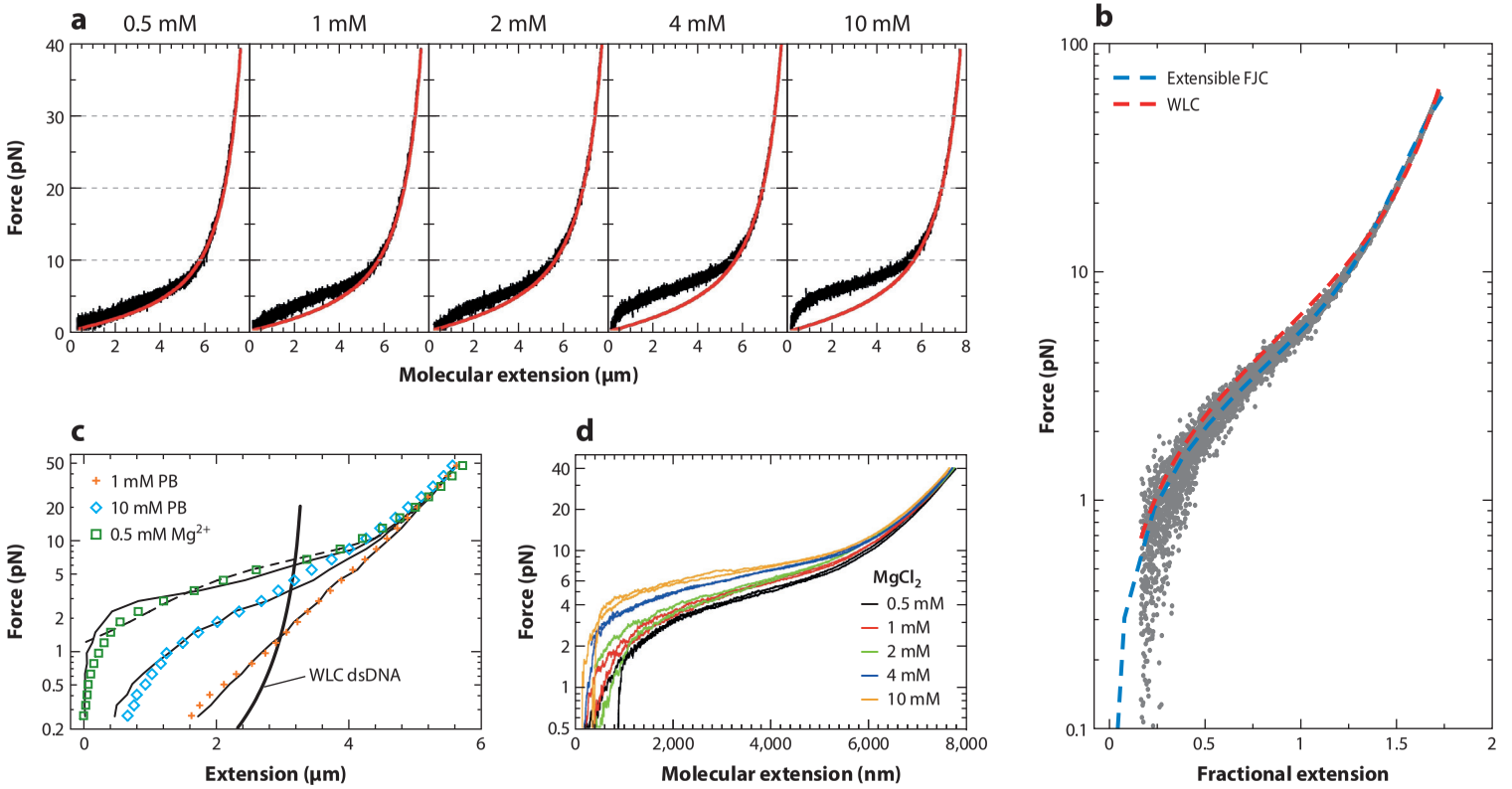

Figure 6

Salt dependence of elasticity and secondary structure formation. (*a*) FECs for different divalent (Mg^{2+}) ionic conditions. Continuous lines are WLC fits to the data. (*b*) Both the WLC and the extensible-FJC models can fit the FEC of ssDNA in the high-force regime. (*c*) Secondary structure formation in different salt conditions measured with magnetic tweezers; dsDNA elasticity is shown for comparison. Modified from Reference 29 with permission. (*d*) Salt dependence of secondary structure formation. Increasing salt concentration stabilizes nonnative secondary structures, leading to a higher force plateau. Abbreviations: dsDNA, double-stranded DNA; FEC, force-extension curve; FJC, freely jointed chain; ssDNA, single-stranded DNA; WLC, worm-like chain.

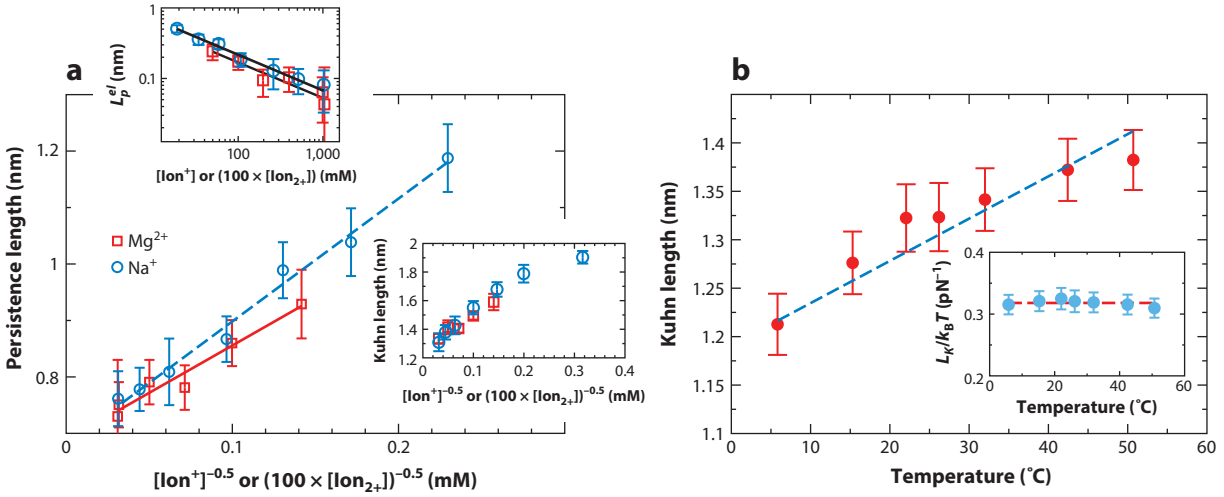

Figure 7

Salt and temperature dependence of the persistence and Kuhn lengths in long ssDNA molecules. (*a*) Salt dependence of the persistence length of ssDNA obtained from fits to the WLC model. *Upper inset:* Scaling of the electrostatic contribution to persistence length. *Lower inset:* Salt dependence of the Kuhn length obtained from a fit to the extensible-FJC model. (*b*) Temperature dependence of the Kuhn length obtained from fits to the extensible-FJC model. Abbreviations: FEC, force-extension curve; FJC, freely jointed chain; ssDNA, single-stranded DNA; WLC, worm-like chain.

The temperature dependence of the elastic properties of ssDNA has also been studied with magnetic and optical tweezers. Early studies with magnetic tweezers found a constant Kuhn length below 10 pN and 40°C, and a reduction in extension not consistent with a constant Kuhn length above 40°C was reported (27). Recently, such measurements have been also performed with a new temperature-jump optical trap (28). In conflict with earlier results, but in accordance with electrostatic theories, the persistence length was found to increase with temperature. However, it is difficult to establish the exact dependence of persistence length on temperature. Temperature can be varied from 5°C to 40°C, which is less than 15% in terms of absolute temperature, much less than the two to three orders of magnitude over which salt concentration can be varied.

According to the WLC model (see Elastic Models for DNA, above), $L_P = A/k_BT$, where A is the bending stiffness. If A is taken to be temperature independent, the model predicts that L_P is inversely proportional to temperature. On the other hand, the FJC model is based on constant (i.e., temperature independent) Kuhn length. As reported above, such results are not compatible with currently available experimental data demonstrating that ideal elastic models are purely phenomenological. Put together, these results suggest that the dependence of the elastic parameters on salt and temperature is primarily of electrostatic origin, explaining why for ssDNA the persistence length increases (rather than decreases) with temperature.

Multivalent cations such as spermidine and dendrimers condense dsDNA; their effect on ssDNA is less well known (5, 64, 79). One might expect the effect to be similar to that observed in proteins that bind to ssDNA, changing not only the elastic properties but also inducing condensation (7, 38). Optical tweezers experiments have shown that cationic hydrophobic peptides can condense both dsDNA and ssDNA, but that condensation of ssDNA can happen at higher stretching forces owing to its lower bending stiffness, facilitating the formation of compact nucleic acid–peptide complexes (19). An interesting characteristic of polycationic ligands that

condense ssDNA is that some of them also facilitate the reannealing of ssDNA, probably by bringing complementary strands close to each other, a feature also observed in polycationic nucleic acid chaperones and SMC (structural maintenance of chromosomes) proteins (14, 19, 66, 82).

BEYOND SIMPLE ELASTIC MODELS

Simple elastic models predict that the force is a sole function of the molecular extension relative to the contour length. However, several studies in dsDNA and ssDNA have reported deviations from this prediction. For dsDNA, the persistence length L_p obtained from fits to the WLC model decreases with the contour length L of the molecule (31, 62, 70). For dsDNA molecules of several thousand base pairs the persistence length can range from 45 to 55 nm, whereas for shorter molecules (a few hundred base pairs) it decreases to 30 nm (70). Noise measurements of very short tethers (58 bp) are much lower, approximately 2 nm (31). The physical significance of these results has been questioned, as the elastic rod model in the continuum limit makes sense only for $L \gg L_p$, and when L is comparable to L_p, finite-size effects should be considered. That the value $L_p = 50$ nm corresponds to approximately 150 bp suggests there might already be corrections for molecules of a few hundred base pairs. Finite-size effects depend on the specific type of boundary condition. In a pulling experiment, the extremities of the molecule are fixed to one bead (single trap setup) or two beads (double trap setup). Thermal forces move and rotate beads in optical and magnetic traps, inducing boundary effects not included in the simplest models. In a recent theoretical and experimental study, Betterton, Perkins, and coworkers (70) demonstrated that for dsDNA molecules L_p decreases with L following the phenomenological scaling formula:

$$L_p(L) = \frac{L_P^\infty}{1 + a\frac{L_P^\infty}{L}}, \qquad 3.$$

where L_P^∞ is the bare persistence length and a is a constant of order 1 that depends on the specific boundary conditions. For dsDNA in standard conditions most studies report that $L_P^\infty = 49 \pm 2$ nm, with $a = 2.78 \pm 0.12$ in single trap optical tweezers studies (22, 70) and $a = 4 \pm 2$ nm in double trap optical tweezers studies (62). Boundary conditions differ in the two cases: In the single trap setup the ends of the DNA are attached to a bead and a surface, whereas in the double trap setup the ends are attached to beads only. Additional finite-size effects that contribute to the L_p value might be the stiffness of hidden compliances along the molecular construct (e.g., the biotin-streptavidin and dig-antidig attachments) that become relevant at short contour lengths. This effect should also lead to lower L_p values for shorter molecules for which it is difficult to separate boundary effects from the stiffness of the attachments. The latter has been estimated to be on the order of 1 pN/nm (31), a value typical of nanometer-sized flexible bond attachments in the range where finite-size effects are observable.

Finite-size effects on the persistence length for other polymers such as microtubules have also been reported (60). In contrast, systematic studies for ssDNA are missing. The main difference between ssDNA and dsDNA is that the former has a much lower persistence length, so finite-size effects should accordingly be smaller (c.f. Equation 3). In spite of the lack of systematic studies, experiments with short and long ssDNA differ. In contrast to the dsDNA, ssDNA is found to be stiffer in experiments on short ssDNA (10–70 bases) than on long ssDNA (1.3–48 kb) (see **Table 1**). For example, force-extension measurements with the oligo method and short-hairpin DNA-unzipping experiments show that L_p changes from 0.7 nm for several kilobases up to 1.1–1.3 nm for just a few tens of bases (2, 3, 12, 83, 84). Similar values were obtained in FRET and AFM imaging experiments (57, 65). These results are difficult to reconcile unless the dimensionless constant a takes a negative value in Equation 3, something not predicted by existing theories.

The interpretation of these results remains open. Using FRET to study 40-base polydT and polyU oligos, Chen et al. (21) suggest that short single-stranded nucleic acids become stiffer in the presence of flanking duplex regions. Although further experiments are needed to clarify these effects, a stiffening of ssDNA in the vicinity of dsDNA regions could explain the discrepancy observed in force spectroscopy measurements, as dsDNA handles are typically used in these experiments.

OPEN QUESTIONS

The mechanics of nucleic acid elasticity has been debated since research in the single-molecule field began. Precise knowledge of the elastic response of nucleic acids is crucial for all single-molecule studies in which the molecular extension is the reaction coordinate: from measuring the translocation of nucleic acid–associated motors to determining the free energy of molecular structures. Several aspects in the field require further investigation, including the dependence of the persistence length on environmental conditions such as salt, temperature, and contour length, and other effects relevant to in vivo conditions such as secondary structure formation and macromolecular crowding. Particularly interesting and much less known are sequence-dependent effects. dsDNA exhibits sequence-dependent bending properties, e.g., the most flexible TATA regions. Although the specific elastic map between sequences and bending rigidities is not known, it is widely surmised that sequence-dependent variability of dsDNA bending stiffness limits the validity of the homogeneous elastic rod model. In general sequence-dependent effects on dsDNA elasticity should be associated with specific short fragments along the molecule that we call specific bending motifs. These motifs are expected to be much smaller than the persistence length of 150 bp. Therefore, unless the dsDNA is too short (a few base pairs), the contribution of sequence-dependent effects to the overall persistence length should be small. In other words, the different stiffnesses of the specific bending motifs do average out along the 50 nm (150 bp) of the generally reported persistence length. In contrast, the low persistence length in ssDNA is comparable to the length of the specific bending motifs, and the contribution of such motifs to the effective persistence length should be much larger. This fact could also explain why L_p decreases when L increases in ssDNA (see Beyond Simple Elastic Models, above). For larger L it is more probable to find low-stiffness specific bending motifs along the sequence. The stiffness of ssDNA is dominated by the low-stiffness motifs: the larger the contour length, the larger the probability to encounter such low-stiffness motifs. This leads to lower persistence length values for larger contour lengths, in accordance with observations. Disorder should also be present for RNA for which sequence-dependent elasticity effects have been reported (71, 72); however, it remains to be determined whether and how the persistence length of RNA depends on its contour length.

DISCLOSURE STATEMENT

The authors are not aware of any affiliations, memberships, funding, or financial holdings that might be perceived as affecting the objectivity of this review.

LITERATURE CITED

1. Abels J, Moreno-Herrero F, Van der Heijden T, Dekker C, Dekker N. 2005. Single-molecule measurements of the persistence length of double-stranded RNA. *Biophys. J.* 88:2737–44
2. Alemany A, Mossa A, Junier I, Ritort F. 2012. Experimental free-energy measurements of kinetic molecular states using fluctuation theorems. *Nat. Phys.* 8:688–94

3. Alemany A, Ritort F. 2014. Determination of the elastic properties of short ssDNA molecules by mechanically folding and unfolding DNA hairpins. *Biopolymers* 101:1193–99
4. Barrat JL, Joanny JF. 1993. Persistence length of polyelectrolyte chains. *Europhys. Lett.* 24:333
5. Baumann CG, Bloomfield VA, Smith SB, Bustamante C, Wang MD, Block SM. 2000. Stretching of single collapsed DNA molecules. *Biophys. J.* 78:1965–78
6. Baumann CG, Smith SB, Bloomfield VA, Bustamante C. 1997. Ionic effects on the elasticity of single DNA molecules. *PNAS* 94:6185–90
7. Bell JC, Liu B, Kowalczykowski SC. 2015. Imaging and energetics of single ssb-ssDNA molecules reveal intramolecular condensation and insight into RecOR function. *eLife* pii:e08646
8. Berndsen ZT, Keller N, Grimes S, Jardine PJ, Smith DE. 2014. Nonequilibrium dynamics and ultraslow relaxation of confined DNA during viral packaging. *PNAS* 111:8345–50
9. Bizarro CV, Alemany A, Ritort F. 2012. Non-specific binding of Na^+ and Mg^{2+} to RNA determined by force spectroscopy methods. *Nucleic Acids Res.* 40:6922–35
10. Bockelmann U, Thomen P, Essevaz-Roulet B, Viasnoff V, Heslot F. 2002. Unzipping DNA with optical tweezers: high sequence sensitivity and force flips. *Biophys. J.* 82:1537–53
11. Bonnet G, Krichevsky O, Libchaber A. 1998. Kinetics of conformational fluctuations in DNA hairpin-loops. *PNAS* 95:8602–6
12. Bosco A, Camunas-Soler J, Ritort F. 2014. Elastic properties and secondary structure formation of single-stranded DNA at monovalent and divalent salt conditions. *Nucleic Acids Res.* 42:2064–74
13. Bouchiat C, Wang M, Allemand J, Strick T, Block S, Croquette V. 1999. Estimating the persistence length of a worm-like chain molecule from force-extension measurements. *Biophys. J.* 76:409–13
14. Braun S, Humphreys C, Fraser E, Brancale A, Bochtler M, Dale T. 2011. Amyloid-associated nucleic acid hybridisation. *PLOS ONE* 6:e19125
15. Brower-Toland BD, Smith CL, Yeh RC, Lis JT, Peterson CL, Wang MD. 2002. Mechanical disruption of individual nucleosomes reveals a reversible multistage release of DNA. *PNAS* 99:1960–65
16. Bryant Z, Oberstrass FC, Basu A. 2012. Recent developments in single-molecule DNA mechanics. *Curr. Opin. Struct. Biol.* 22:304–12
17. Bustamante C, Bryant Z, Smith SB. 2003. Ten years of tension: single-molecule DNA mechanics. *Nature* 421:423–27
18. Bustamante C, Smith SB, Liphardt J, Smith D. 2000. Single-molecule studies of DNA mechanics. *Curr. Opin. Struct. Biol.* 10:279–85
19. Camunas-Soler J, Frutos S, Bizarro CV, de Lorenzo S, Fuentes-Perez ME, et al. 2013. Electrostatic binding and hydrophobic collapse of peptide–nucleic acid aggregates quantified using force spectroscopy. *ACS Nano* 7:5102–13
20. Candelli A, Hoekstra TP, Farge G, Gross P, Peterman EJ, Wuite GJ. 2013. A toolbox for generating single-stranded DNA in optical tweezers experiments. *Biopolymers* 99:611–20
21. Chen H, Meisburger SP, Pabit SA, Sutton JL, Webb WW, Pollack L. 2012. Ionic strength-dependent persistence lengths of single-stranded RNA and DNA. *PNAS* 109:799–804
22. Chen YF, Wilson DP, Raghunathan K, Meiners JC. 2009. Entropic boundary effects on the elasticity of short DNA molecules. *Phys. Rev. E* 80:020903
23. Clausen-Schaumann H, Rief M, Tolksdorf C, Gaub HE. 2000. Mechanical stability of single DNA molecules. *Biophys. J.* 78:1997–2007
24. Cluzel P, Lebrun A, Heller C, Lavery R, Viovy JL, et al. 1996. DNA: an extensible molecule. *Science* 271:792–94
25. Dame RT, Noom MC, Wuite GJ. 2006. Bacterial chromatin organization by H-NS protein unravelled using dual DNA manipulation. *Nature* 444:387–90
26. Danilowicz C, Coljee VW, Bouzigues C, Lubensky DK, Nelson DR, Prentiss M. 2003. DNA unzipped under a constant force exhibits multiple metastable intermediates. *PNAS* 100:1694–99
27. Danilowicz C, Lee C, Coljee V, Prentiss M. 2007. Effects of temperature on the mechanical properties of single stranded DNA. *Phys. Rev. E* 75:030902
28. de Lorenzo S, Ribezzi-Crivellari M, Arias-Gonzalez JR, Smith SB, Ritort F. 2015. A temperature-jump optical trap for single-molecule manipulation. *Biophys. J.* 108:2854–64

29. Dessinges MN, Maier B, Zhang Y, Peliti M, Bensimon D, Croquette V. 2002. Stretching single stranded DNA, a model polyelectrolyte. *Phys. Rev. Lett.* 89:248102
30. Dršata T, Špačková N, Jurečka P, Zgarbová M, Šponer J, Lankaš F. 2014. Mechanical properties of symmetric and asymmetric DNA A-tracts: implications for looping and nucleosome positioning. *Nucleic Acids Res.* 42:7383–94
31. Forns N, de Lorenzo S, Manosas M, Hayashi K, Huguet JM, Ritort F. 2011. Improving signal/noise resolution in single-molecule experiments using molecular constructs with short handles. *Biophys. J.* 100:1765–74
32. Forth S, Deufel C, Sheinin MY, Daniels B, Sethna JP, Wang MD. 2008. Abrupt buckling transition observed during the plectoneme formation of individual DNA molecules. *Phys. Rev. Lett.* 100:148301
33. Fu H, Chen H, Marko JF, Yan J. 2010. Two distinct overstretched DNA states. *Nucleic Acids Res.* 38(16):5594–600
34. Fu H, Chen H, Zhang X, Qu Y, Marko JF, Yan J. 2010. Transition dynamics and selection of the distinct s-DNA and strand unpeeling modes of double helix overstretching. *Nucleic Acids Res.* 39(8):3473–81
35. Goddard NL, Bonnet G, Krichevsky O, Libchaber A. 2000. Sequence dependent rigidity of single stranded DNA. *Phys. Rev. Lett.* 85:2400
36. Gross P, Laurens N, Oddershede LB, Bockelmann U, Peterman EJ, Wuite GJ. 2011. Quantifying how DNA stretches, melts and changes twist under tension. *Nat. Phys.* 7:731–36
37. Hall MA, Shundrovsky A, Bai L, Fulbright RM, Lis JT, Wang MD. 2009. High-resolution dynamic mapping of histone-DNA interactions in a nucleosome. *Nat. Struct. Mol. Biol.* 16:124–29
38. Hamon L, Pastre D, Dupaigne P, Le Breton C, Le Cam E, Pietrement O. 2007. High-resolution AFM imaging of single-stranded DNA-binding (ssb) protein-DNA complexes. *Nucleic Acids Res.* 35:e58
39. Herrero-Galán E, Fuentes-Perez ME, Carrasco C, Valpuesta JM, Carrascosa JL, et al. 2012. Mechanical identities of RNA and DNA double helices unveiled at the single-molecule level. *J. Am. Chem. Soc.* 135:122–31
40. Huguet JM, Bizarro CV, Forns N, Smith SB, Bustamante C, Ritort F. 2010. Single-molecule derivation of salt dependent base-pair free energies in DNA. *PNAS* 107:15431–36
41. Ibarra B, Chemla YR, Plyasunov S, Smith SB, Lazaro JM, et al. 2009. Proofreading dynamics of a processive DNA polymerase. *EMBO J.* 28:2794–802
42. Jacobson DR, McIntosh DB, Saleh OA. 2013. The snakelike chain character of unstructured RNA. *Biophys. J.* 105:2569–76
43. Kauert DJ, Kurth T, Liedl T, Seidel R. 2011. Direct mechanical measurements reveal the material properties of three-dimensional DNA origami. *Nano Lett.* 11:5558–63
44. Ke C, Humeniuk M, Hanna S, Marszalek PE, et al. 2007. Direct measurements of base stacking interactions in DNA by single-molecule atomic-force spectroscopy. *Phys. Rev. Lett.* 99:018302
45. Keyser UF, Koeleman BN, Van Dorp S, Krapf D, Smeets RM, et al. 2006. Direct force measurements on DNA in a solid-state nanopore. *Nat. Phys.* 2:473–77
46. Kim DN, Kilchherr F, Dietz H, Bathe M. 2012. Quantitative prediction of 3D solution shape and flexibility of nucleic acid nanostructures. *Nucleic Acids Res.* 40:2862–68
47. Kratky O, Porod G. 1949. Röntgenuntersuchung gelöster fadenmoleküle. *Recl. Trav. Chim. Pays-Bas* 68:1106–22
48. Landau LD, Lifshitz EM. 1982. *Mechanics*, Volume 1: *Course of Theoretical Physics, 3rd Edition*. Oxford, UK: Elsevier
49. Lionnet T, Dawid A, Bigot S, Barre FX, Saleh OA, et al. 2006. DNA mechanics as a tool to probe helicase and translocase activity. *Nucleic Acids Res.* 34:4232–44
50. Manosas M, Perumal SK, Croquette V, Benkovic SJ. 2012. Direct observation of stalled fork restart via fork regression in the T4 replication system. *Science* 338:1217–20
51. Manosas M, Xi XG, Bensimon D, Croquette V. 2010. Active and passive mechanisms of helicases. *Nucleic Acids Res.* 38(16):5518–26
52. Marko JF, Siggia ED. 1995. Stretching DNA. *Macromolecules* 28:8759–70
53. Marszalek PE, Oberhauser AF, Pang YP, Fernandez JM. 1998. Polysaccharide elasticity governed by chair–boat transitions of the glucopyranose ring. *Nature* 396:661–64
54. McGurn A, Scalapino D. 1975. One-dimensional ferromagnetic classical-spin-field model. *Phys. Rev. B* 11:2552

55. McIntosh DB, Duggan G, Gouil Q, Saleh OA. 2014. Sequence-dependent elasticity and electrostatics of single-stranded DNA: signatures of base-stacking. *Biophys. J.* 106:659–66
56. McIntosh DB, Saleh OA. 2011. Salt species-dependent electrostatic effects on ssDNA elasticity. *Macromolecules* 44:2328–33
57. Murphy M, Rasnik I, Cheng W, Lohman TM, Ha T. 2004. Probing single-stranded DNA conformational flexibility using fluorescence spectroscopy. *Biophys. J.* 86:2530–37
58. Nelson P. 2004. *Biological Physics*. New York: Freeman
59. Odijk T. 1977. Polyelectrolytes near the rod limit. *J. Polymer Sci.* 15:477–83
60. Pampaloni F, Lattanzi G, Jonáš A, Surrey T, Frey E, Florin EL. 2006. Thermal fluctuations of grafted microtubules provide evidence of a length-dependent persistence length. *PNAS* 103:10248–53
61. Pfitzner E, Wachauf C, Kilchherr F, Pelz B, Shih WM, et al. 2013. Rigid DNA beams for high-resolution single-molecule mechanics. *Angew. Chem. Int. Ed. Engl.* 125:7920–25
62. Ribezzi-Crivellari M, Ritort F. 2012. Force spectroscopy with dual-trap optical tweezers: molecular stiffness measurements and coupled fluctuations analysis. *Biophys. J.* 103:1919–28
63. Rief M, Pascual J, Saraste M, Gaub HE. 1999. Single molecule force spectroscopy of spectrin repeats: low unfolding forces in helix bundles. *J. Mol. Biol.* 286:553–61
64. Ritort F, Mihardja S, Smith SB, Bustamante C. 2006. Condensation transition in DNA-polyaminoamide dendrimer fibers studied using optical tweezers. *Phys. Rev. Lett.* 96:118301
65. Rivetti C, Walker C, Bustamante C. 1998. Polymer chain statistics and conformational analysis of DNA molecules with bends or sections of different flexibility. *J. Mol. Biol.* 280:41–59
66. Sakai A, Hizume K, Sutani T, Takeyasu K, Yanagida M. 2003. Condensin but not cohesin SMC heterodimer induces DNA reannealing through protein–protein assembly. *EMBO J.* 22:2764–75
67. Saleh OA. 2015. Single polymer mechanics across the force regimes. *J. Chem. Phys.* 142:194902
68. Saleh OA, McIntosh DB, Pincus P, Ribeck N. 2009. Nonlinear low-force elasticity of single-stranded DNA molecules. *Phys. Rev. Lett.* 102:068301
69. SantaLucia J. 1998. A unified view of polymer, dumbbell, and oligonucleotide DNA nearest-neighbor thermodynamics. *PNAS* 95:1460–65
70. Seol Y, Li J, Nelson PC, Perkins TT, Betterton M. 2007. Elasticity of short DNA molecules: theory and experiment for contour lengths of 0.6–7 μm. *Biophys. J.* 93:4360–73
71. Seol Y, Skinner GM, Visscher K. 2004. Elastic properties of a single-stranded charged homopolymeric ribonucleotide. *Phys. Rev. Lett.* 93:118102
72. Seol Y, Skinner GM, Visscher K, Buhot A, Halperin A. 2007. Stretching of homopolymeric RNA reveals single-stranded helices and base-stacking. *Phys. Rev. Lett.* 98:158103
73. Shundrovsky A, Smith CL, Lis JT, Peterson CL, Wang MD. 2006. Probing SWI/SNF remodeling of the nucleosome by unzipping single DNA molecules. *Nat. Struct. Mol. Biol.* 13:549–54
74. Skolnick J, Fixman M. 1977. Electrostatic persistence length of a wormlike polyelectrolyte. *Macromolecules* 10:944–48
75. Smith DE, Tans SJ, Smith SB, Grimes S, Anderson DL, Bustamante C. 2001. The bacteriophage φ29 portal motor can package DNA against a large internal force. *Nature* 413:748–52
76. Smith SB, Cui Y, Bustamante C. 1996. Overstretching b-DNA: the elastic response of individual double-stranded and single-stranded DNA molecules. *Science* 271:795–99
77. Smith SB, Finzi L, Bustamante C. 1992. Direct mechanical measurements of the elasticity of single DNA molecules by using magnetic beads. *Science* 258:1122–26
78. Strick T, Allemand JF, Bensimon D, Bensimon A, Croquette V. 1996. The elasticity of a single supercoiled DNA molecule. *Science* 271:1835–37
79. Todd BA, Rau DC. 2008. Interplay of ion binding and attraction in DNA condensed by multivalent cations. *Nucleic Acids Res.* 36:501–10
80. van der Heijden T, Modesti M, Hage S, Kanaar R, Wyman C, Dekker C. 2008. Homologous recombination in real time: DNA strand exchange by RECA. *Mol. Cell* 30:530–38

81. Wang MD, Yin H, Landick R, Gelles J, Block SM. 1997. Stretching DNA with optical tweezers. *Biophys. J.* 72:1335
82. Williams MC, Rouzina I, Bloomfield VA. 2002. Thermodynamics of DNA interactions from single molecule stretching experiments. *Acc. Chem. Res.* 35:159–66
83. Woodside MT, Anthony PC, Behnke-Parks WM, Larizadeh K, Herschlag D, Block SM. 2006. Direct measurement of the full, sequence-dependent folding landscape of a nucleic acid. *Science* 314:1001–4
84. Woodside MT, Behnke-Parks WM, Larizadeh K, Travers K, Herschlag D, Block SM. 2006. Nanomechanical measurements of the sequence-dependent folding landscapes of single nucleic acid hairpins. *PNAS* 103:6190–95

Annual Review of Biophysics
Volume 45, 2016

Contents

Indexes

Errata

An online log of corrections to *Annual Review of Biophysics* articles may be found at http://www.annualreviews.org/errata/biophys